

# Estimation of land surface window (8–12 $\mu\text{m}$ ) emissivity from multi-spectral thermal infrared remote sensing — A case study in a part of Sahara Desert

Kenta Ogawa, Thomas Schmugge, and Frederic Jacob  
USDA/ARS Hydrology and Remote Sensing Lab, Beltsville, MD, USA

Andrew French

Hydrological Science Branch, NASA Goddard Space Flight Center, Greenbelt, MD, USA

Received 27 September 2002; revised 8 November 2002; accepted 6 December 2002; published XX Month 2003.

[1] Land surface window emissivity is an important parameter for estimating the longwave radiative budget. This study focuses on estimating the window (8–12  $\mu\text{m}$ ) emissivity from the waveband emissivities of the five thermal infrared channels of the Advanced Spaceborne Thermal Emission and Reflection Radiometer (ASTER). ASTER data along with the Temperature-Emissivity Separation (TES) algorithm allows us to estimate surface channel emissivities with 90 m spatial resolution globally. Multiple regression was used to relate window emissivity to the five ASTER emissivities. This regression was developed using spectral libraries. Its residual error was less than 0.005 (RMSE) for values ranging between 0.81 and 1.00. We applied this regression to ASTER emissivities extracted from data acquired in 2001 and 2002 over a  $240 \times 1200$  km area in a desert of North Africa. A comparison against a classification based emissivity map showed significant differences ranging between  $-0.08$  and  $+0.06$ . INDEX TERMS: 1640 Global Change: Remote sensing; 1878 Hydrology: Water/energy interactions; 9305 Information Related to Geographic Region: Africa. Citation: Ogawa, K., T. Schmugge, F. Jacob, and A. French, Estimation of land surface window (8–12  $\mu\text{m}$ ) emissivity from multi-spectral thermal infrared remote sensing — A case study in a part of Sahara Desert, *Geophys. Res. Lett.*, 30(0), XXXX, doi:10.1029/2002GL016354, 2003.

## 1. Introduction

[2] Surface window emissivity is an important parameter for the estimation of the surface radiation budget. For clear-sky condition a large part of the total radiative emission from earth is directly lost into space within this window region, knowledge of the surface emissivity at these wavelengths is critical in earth-atmosphere system radiation budget studies. However the window emissivity (8–12  $\mu\text{m}$ :  $1250\text{--}833\text{ cm}^{-1}$ ) can vary significantly, because the spectral emissivity varies between 0.65 and 1.0 for bare soils and rocks in this range [Salisbury and D’Aria, 1992]. Estimating surface emissivity with an error of 10% yields significant inaccuracy on the amount of radiation loss to space [Prabhakara and Dalu, 1976]. Surface emissivity and longwave net surface radiation are proportional, thus a 10% variation of emissivity induces a 10% change in longwave net radiation. Both regional and global climate models are

particularly sensitive to these radiation effects since they depend on the surface radiation budget (Presented by Zhang H.Y. and W.L. Smith, “The spectral variation of surface emissivity within the 8–12  $\mu\text{m}$  “Window”, at AGU Fall Meeting in 1990).

[3] However, in model parameterization for land surface energy balance studies and numerical weather predictions, a constant and uniform emissivity is often used [Wood *et al.*, 1998; Blondin, 1991] because of the limited knowledge about spatial variation of emissivity. Wilber *et al.* [1999] generated a global window emissivity map using both land classification maps [Belward and Loveland, 1996] and corresponding emissivity values calculated from spectral libraries [Salisbury and D’Aria, 1992]. The advantage of this method is the possibility of obtaining maps at a global scale. However, large spatial variations of emissivity can be observed in rocks and soils, which are recognized to be one surface type, such as barren, desert or bare soils in classification maps. Prabhakara and Dalu [1976] mapped the surface emissivity with 100 km resolution using NIMBUS-4 InfraRed Interferometer Spectrometer (IRIS). A map with finer spatial resolution, such as 90 m resolution provided by the ASTER sensor [Yamaguchi *et al.*, 1998], will be useful for surface energy balance studies at local scales and for the validation of coarse resolution maps. ASTER is a sensor onboard the Earth Observing System (EOS) Terra satellite launched in 1999, and has five channels in the thermal infrared region (8–12  $\mu\text{m}$ ). It is possible to estimate spectral emissivity of the five channel using Temperature-Emissivity Separation (TES) algorithm.

[4] In this study, we express the window emissivity as a linear combination of the five channel emissivities from ASTER data. This approach is similar to the broadband emissivity (3–14  $\mu\text{m}$ ) estimation [Ogawa *et al.*, 2002]. We calibrated and validated a regression using a dataset of both window and ASTER emissivities generated using spectral libraries. We applied this regression to ASTER emissivities over a  $240 \times 1200$  km area in northern Sahara Desert and compared the ASTER window emissivity map with a classification based emissivity map.

## 2. Method

[5] We found that window emissivity  $\epsilon_{8-12}$  can be expressed as a linear combination of ASTER channel emissivities  $\epsilon_{ch,n}$  (The center wavelengths of ASTER chan-

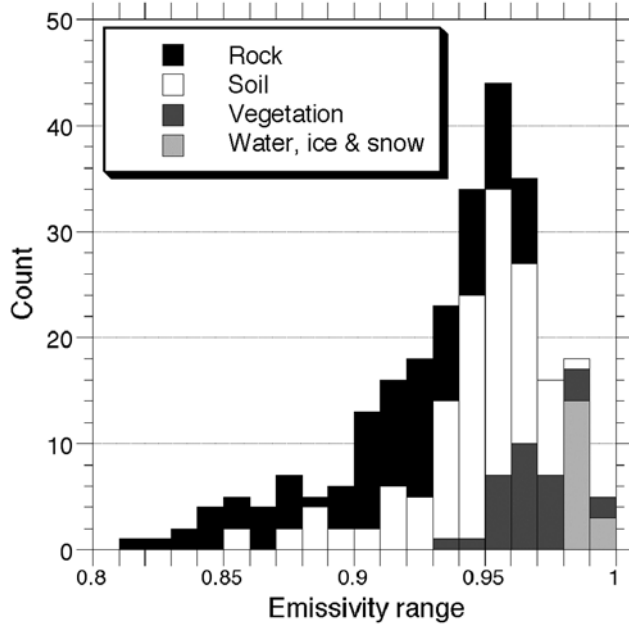


**Figure 1.** Histogram of window emissivity (8–12  $\mu\text{m}$ ),  $\varepsilon_{8-12}$  calculated from spectral libraries of total 257 samples. The collection includes 113 soil types, 31 vegetation types, 96 rock types, and 17 water types.

nels 10 to 14 are 8.29, 8.63, 9.08, 10.66, 11.29  $\mu\text{m}$ , respectively):

$$\varepsilon_{8-12} = \sum_{ch=10}^{14} a_{ch}\varepsilon_{ch,n} + c \quad (1)$$

Where  $a_{ch}$  and  $c$  are coefficients obtained using linear regression, and  $\varepsilon_{8-12}$  are defined as:

$$\varepsilon_{8-12} \equiv \frac{\int_{\lambda=8}^{\lambda=12} \varepsilon(\lambda)B(\lambda, T)d\lambda}{\int_{\lambda=8_1}^{\lambda=12} B(\lambda, T)d\lambda} \quad (2)$$

Where  $\varepsilon(\lambda)$  is spectral emissivity at the wavelength  $\lambda$ ,  $B$  is the Planck function, and  $T$  is surface temperature. The ASTER channel  $n$  emissivities  $\varepsilon_{ch,n}$  are defined using the sensor spectral response function  $f_{ch,n}(\lambda)$  as:

$$\varepsilon_{ch,n} \equiv \frac{\int f_{ch,n}(\lambda)\varepsilon(\lambda)B(\lambda, T)d\lambda}{\int f_{ch,n}(\lambda)B(\lambda, T)d\lambda} \quad (3)$$

[6] We used two spectral libraries for the calibration and validation of (1). For calibration, we selected 150 spectra collected by *Salisbury and D’Aria* [1992] at Johns Hopkins

**Table 1.** Calibrated Coefficients of (1) Obtained Using JHU/ASTER Spectral Library

$a_{10}$	$a_{11}$	$a_{12}$	$a_{13}$	$a_{14}$	$C$
0.014	0.145	0.241	0.467	0.004	0.128

**Table 2.** The Error and Range of Window Emissivity in Calibration and Validation

Error (RMSE)	Maximum error	Range
Calibration using JHU/ASTER library		
0.0048	0.022	0.81–1.00
Validation using UCSB library		
0.0040	0.020	0.85–1.00

Bias: + 0.0003 (in validation)

University (JHU) from the ASTER Spectral library because it has larger emissivity range. For validation we selected 107 spectra collected by *Snyder et al.* [1997] at the University of California, Santa Barbara (UCSB). The JHU library contains directional hemispherical spectral reflectance,  $\rho_\lambda$ , therefore we converted to spectral emissivity  $\varepsilon_\lambda$  using Kirchhoff’s law,  $\varepsilon_\lambda = 1 - \rho_\lambda$ . UCSB library provides emissivity spectra. We assumed that  $T = 300$  K in this analysis.

[7] We calculated  $\varepsilon_{8-12}$  and  $\varepsilon_{ch,10}$  to  $\varepsilon_{ch,14}$  using (2) and (3) for all the samples describe above. The calculated  $\varepsilon_{8-12}$  ranged from 0.81 to 1.00 (Figure 1). The emissivities of rock and soil widely ranged from 0.81 to 0.99. Using calculated  $\varepsilon_{8-12}$  and  $\varepsilon_{ch,10}$  to  $\varepsilon_{ch,14}$  for JHU library, we obtained the coefficients in (1) from using the multiple linear regression (Table 1). And then, we validated the regression using calculated  $\varepsilon_{8-12}$  and  $\varepsilon_{ch,10}$  to  $\varepsilon_{ch,14}$  for UCSB library. Table 2 shows the ranges of emissivities, the RMS and maximum errors in both calibration and validation. Here, the error is the difference between  $\varepsilon_{8-12}$  predicted by (1) and  $\varepsilon_{8-12}$  calculated by (2). RMS errors were less than 0.005. Figure 2 shows the comparison of predicted and calculated values of  $\varepsilon_{8-12}$  for both calibration and validation. The errors were large in ultramafic and

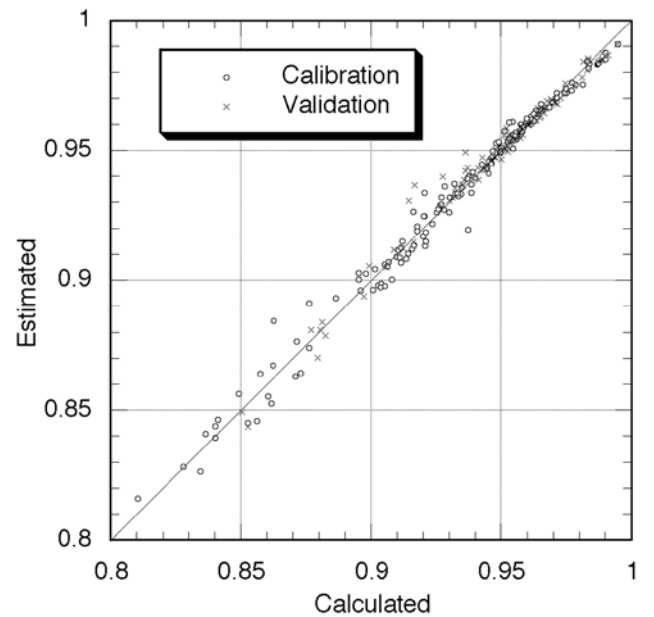


**Figure 2.** Comparison of calculated window emissivity ( $\varepsilon_{8-12}$ ) using (2) and predicted window emissivity using (1) with coefficients of Table 1 in calibration and validation.

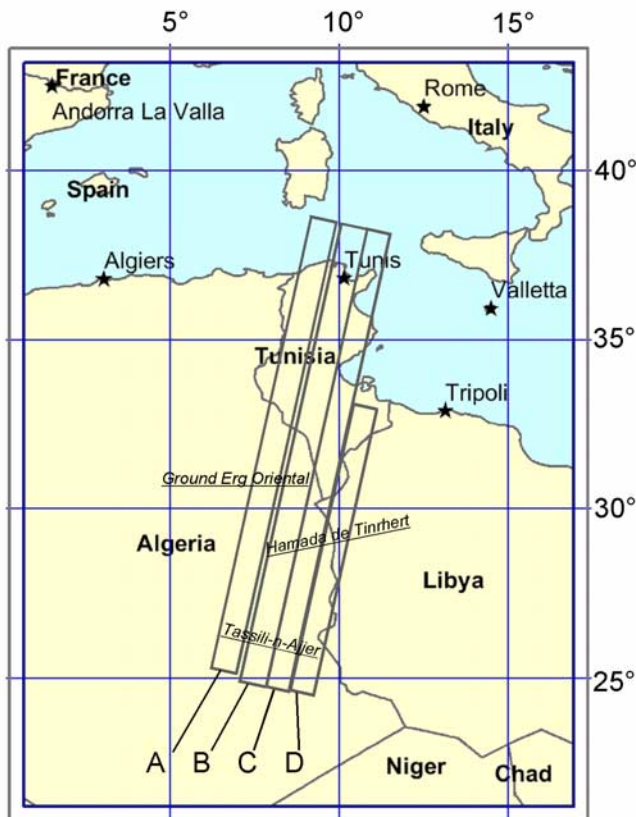


**Figure 3.** Study area over Tunisia and Algeria. A, B, C, D indicate the ASTER paths of data acquisition. The 85 scenes of ASTER data are used to cover this area.

mafic rocks samples, such as picrite. Maximum absolute error is 0.022. Both the RMS and maximum error were larger in calibration than in validation. A possible reason is that only the JHU library includes rock samples, some of which give larger errors. We also tried other empirical functions, such as 1) the linear regression without a constant, and 2) polynomial regression, however we didn't observe significant improvements in either instance. In this analysis, any errors in the ASTER channel emissivities were not considered. The accuracy of ASTER emissivity is estimated to be 0.015 [Gillespie *et al.*, 1998]. Therefore the expected accuracy of window emissivity will be less than 0.02.

### 3. Results and Discussion

[8] We applied the regression for mapping window emissivity and compared it with a classification based emissivity map [Wilber *et al.*, 1999]. As a study area, we selected a  $240 \times 1200$  km over Algeria and Tunisia (Figure 3). This choice was driven by a wide variety of land cover, including sand dunes in the Grand Erg Oriental, mountainous regions in Hamada de Tinrhert, and vegetated areas along with the Mediterranean Sea. ASTER data were acquired in 2000 and 2001 over this region.

[9] We used 85 scenes of ASTER level 2 emissivity product (Table 3) processed at the Earth Resources Observation System (EROS) Data Center (EDC) of the U.S. Geological Survey. The data were atmospherically corrected

**Table 3.** ASTER Data Used in this Study

Path <sup>a</sup>	Date	Location	Number of scenes <sup>b</sup>
A	14 Nov 2001	37.2N–25.6N	23
B	11 Feb 2002	37.4N–25.1N	23
C	15 May 2001	33.5N–25.0N	17
C	31 May 2001	37.3N–33.5N	8
D	19 Aug 2001	31.8N–24.9N	14

<sup>a</sup>Refer Figure 3 for the locations.

<sup>b</sup>Total: 85 scenes.

[Palluconi *et al.*, 1996], and then the TES algorithm [Gillespie *et al.*, 1998] was applied. The emissivity of channel 12 had the widest range (between 0.64 and 1.00), whereas emissivities of channel 13 and 14 had very narrow ranges (Figure 4). The spectra of the west part of Grand Erg Oriental (low value in channel 12) were typical of quartz spectra. The northern area along the Mediterranean Sea had rich vegetation, and therefore it had higher emissivity (0.9–1.0) in all five channels.

[10] The regression (1) with the coefficients given in Table 1 was applied to the ASTER emissivity products

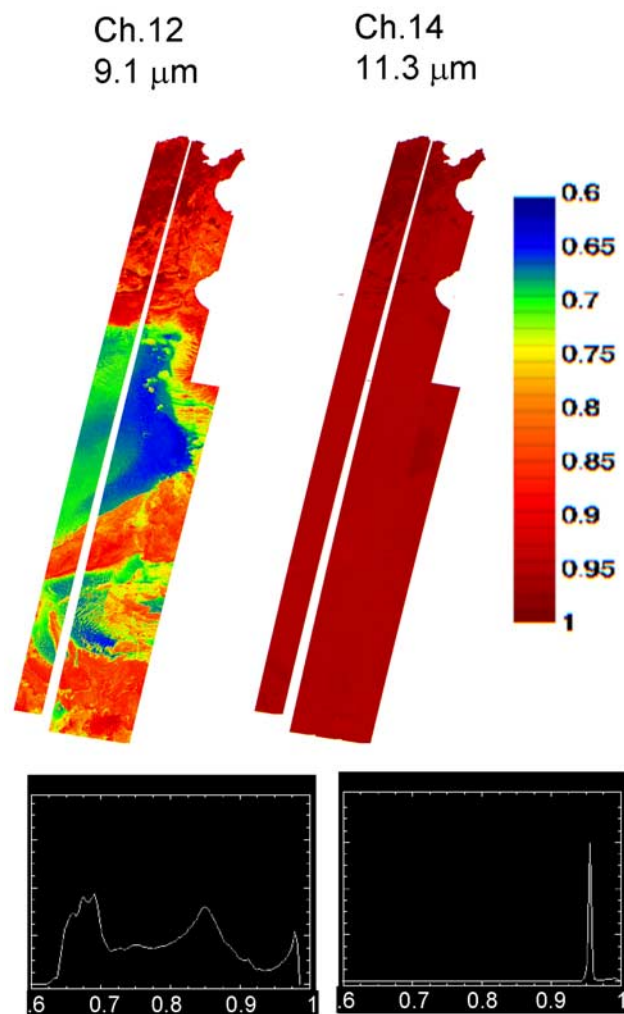


**Figure 4.** Emissivity map of ASTER channel 12, 9.08  $\mu\text{m}$  (which has the largest range of all five channels), and channel 14, 11.29  $\mu\text{m}$  (the smallest range) in study area.

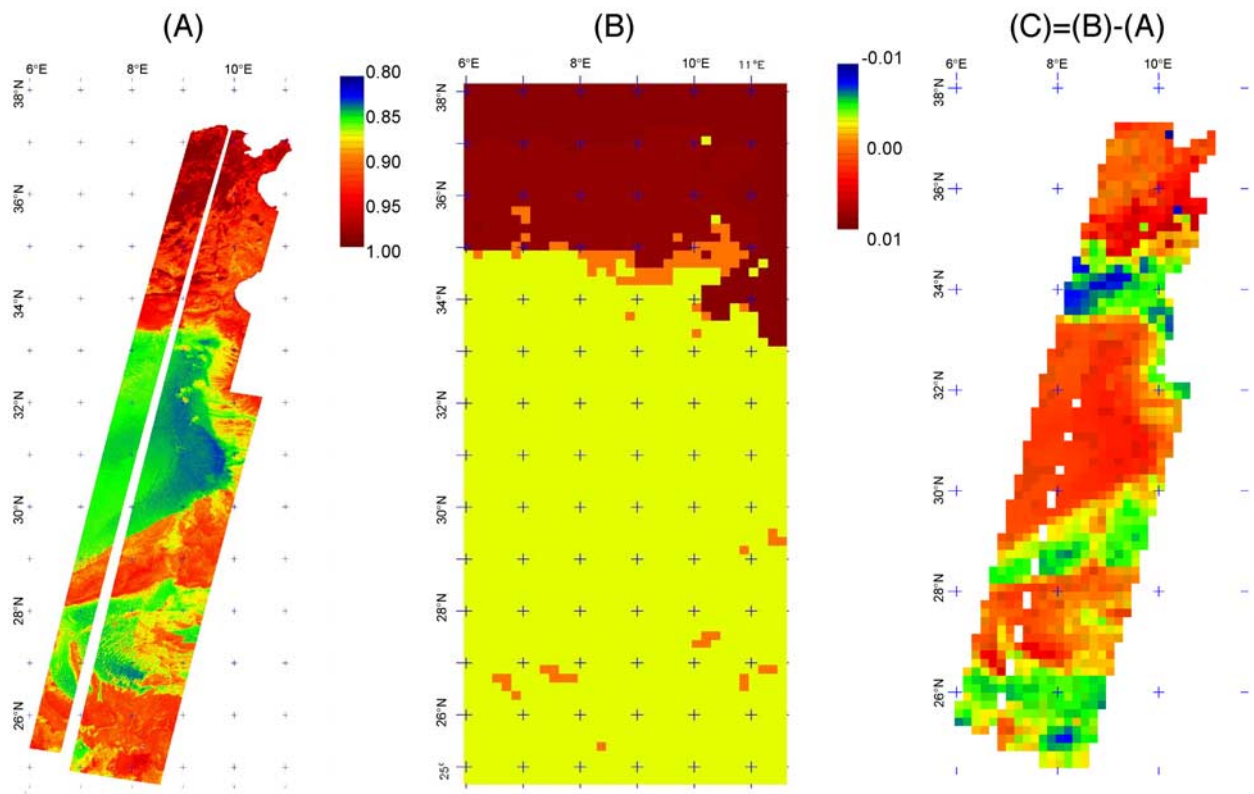


**Figure 5.** (a) Window emissivity map (8–12  $\mu\text{m}$ ) derived from 85 scenes of ASTER data, (b) Classification based emissivity map in 10 minutes resolution [from Wilber *et al.*, 1999], (c) The difference between (a) and (b).

and then a mosaic of the window emissivity map was produced (Figure 5a). Window emissivities ranged from 0.81 to 0.99. Lower emissivities between 0.83 and 0.87 were observed in the sand dunes area in Grand Erg Oriental. Higher emissivities, mostly between 0.89 and 0.94, were observed in the mountainous areas, Hamada de Tinrhert and Tassili-n-Ajjer. Small differences were observed at the borders of Path C and Path D. RMS differences of emissivity values at overlapped area of Path C and Path D ( $\approx 3 \times 1000$  km) were 0.007 for  $\epsilon_{8-12}$  and 0.021 for  $\epsilon_{ch.12}$ . TES itself would not cause these differences if the actual emissivity was stable and atmospheric correction was accurate. The differences probably resulted from temporal variations of emissivity or errors in the atmospheric corrections, most likely the latter. Further study is necessary to identify the cause of differences.

[11] We compared this window emissivity map with the emissivity map from Wilber *et al.* [1999] (Figure 5b). Wilber’s emissivity map is based on a land classification map, and a table of emissivity values for each land use generated using a spectral library. In Figure 5B, low value ( $\approx 0.87$ ), middle value ( $\approx 0.89$ ), and high value ( $\approx 0.96$ ) regions correspond to “Barren/Desert region”, “Open/Shrubs region”, and “Sea Water/Cropland/Savanna/Grassland region” respectively. In the Barren/Desert region, window emissivity derived from ASTER ranged between 0.81 and 0.95 (Figure 5a). As expected from the histogram (Figure 1), the range of the window emissivity for the desert area was large. Significant differences ( $-0.08$  to  $+0.06$ ) between the classification based emis-

sivity map and the ASTER emissivity map were observed (Figure 5c).

#### 4. Conclusion

[12] In this paper, we used a linear regression for estimating window (8–12  $\mu\text{m}$ ) emissivity using the five ASTER channel emissivities. The calibration and validation were done using two independent spectral libraries. We found that the estimation of the window emissivity is potentially accurate and the RMS error was less than 0.005 in calibration and validation (excluding the error in emissivities derived from ASTER data) for emissivities ranging between 0.81 and 1.00.

[13] We applied the regression to 85 scenes of ASTER data acquired over the northern Sahara Desert and created a window emissivity map over a  $240 \times 1200$  km area. We found that there were significant differences (0.08 at maximum) between the classification base window emissivity map and the ASTER emissivity map. These results indicate that ASTER data are useful for the validation of existing emissivity maps and for generating more accurate and higher spatial resolution emissivity maps. Further study is necessary for validating window emissivity derived from ASTER data.

[14] **Acknowledgments.** This study was supported by the ASTER Project of NASA’s EOS-Terra Program. ASTER Spectral Library was provided by the Jet Propulsion Laboratory, California Institute of Technology, Pasadena, California.

## References

- Belward, A., and T. Loveland, The DIS 1-km land cover data set, *Global Change, The IGBP Newsletter*, 27, 1996.
- Blondin, C., Parameterization of land-surface processes in numerical weather prediction, in *Land surface Evaporation*, edited by T. J. Schmugge and J. Andre, pp. 31–54, Springer-Verlag, New York, 1991.
- Gillespie, A., S. Rokugawa, T. Matsunaga, J. S. Cothem, S. Hook, and A. B. Kahle, A temperature and emissivity separation algorithm for Advanced Spaceborne Thermal Emission and Reflection radiometer (ASTER) images, *IEEE Trans. on Geosci. and Remote Sens.*, 36, 1113–1126, 1998.
- Ogawa, K., T. Schmugge, F. Jacob, and A. French, Estimation of Broad-band Land Surface Emissivity from Multi-Spectral Thermal Infrared Remote Sensing, *Agronomie*, 22(6), 695–696, 2002.
- Palluconi, F., G. Hoover, R. Alley, M. J. Nilsen, and T. Thompson, An atmospheric correction method for ASTER thermal radiometry over land, *ASTER Algorithm Theoretical Basis Document (ATBD) revision 2*, Jet Propulsion Lab., Pasadena, CA, 1996.
- Prabhakara, C., and G. Dalu, Remote sensing of the surface emissivity at 9  $\mu\text{m}$  over the globe, *J. Geophys. Res.*, 81(21), 3719–3724, 1976.
- Salisbury, J. W., and D. M. D’Aria, Emissivity of terrestrial materials in the 8–14  $\mu\text{m}$  atmospheric window, *Remote Sens. Environ.*, 42, 83–106, 1992.
- Snyder, W. C., Z. Wan, Y. Zhang, and Y. Feng, Thermal infrared (3–14  $\mu\text{m}$ ) bi-directional reflectance measurement of sands and soils, *Remote Sens. of Environ.*, 60, 101–109, 1997.
- Wilber, A. C., D. P. Kratz, and S. K. Gupta, Surface emissivity maps for use in satellite retrievals of longwave radiation, NASA/TP-1999-209362, pp. 30, 1999.
- Wood, E. F., et al., The project for intercomparison of land-surface parameterization scheme (PILPS) Phase 2(c) Red-Arkansas River basin experiment: 1. Experiment description and summary intercomparisons, *Global and Planetary Change*, 19, 115–135, 1998.
- Yamaguchi, Y., A. B. Kahale, H. Tsu, T. Kawakami, and M. Pniel, Overview of Advanced Spaceborne Thermal Emission and Reflection radiometer (ASTER), *IEEE Trans. on Geosci. and Remote Sens.*, 36, 1062–1071, 1998.

---

K. Ogawa, T. Schmugge, and F. Jacob, USDA/ARS Hydrology and Remote Sensing Lab, Beltsville, MD 20705-2350, USA.

A. French, Hydrological Science Branch, NASA Goddard Space Flight Center, Greenbelt, MD 20771, USA.